



# Differences in the Default Mode Network of Temporal Lobe Epilepsy Patients Detected by Hilbert-Huang Transform Based Dynamic Functional Connectivity

Ye Yuan<sup>1,2</sup> · Ying Duan<sup>3</sup> · Wan Li<sup>4</sup> · Jiechuan Ren<sup>5</sup> · Zhimei Li<sup>5</sup> · Chunlan Yang<sup>1</sup>

Received: 25 April 2022 / Accepted: 15 April 2023 / Published online: 28 April 2023

© The Author(s), under exclusive licence to Springer Science+Business Media, LLC, part of Springer Nature 2023

## Abstract

Resting-state functional connectivity, constructed via functional magnetic resonance imaging, has become an essential tool for exploring brain functions. Aside from the methods focusing on the static state, investigating dynamic functional connectivity can better uncover the fundamental properties of brain networks. Hilbert-Huang transform (HHT) is a novel time–frequency technique that can adapt to both non-linear and non-stationary signals, which may be an effective tool for investigating dynamic functional connectivity. To perform the present study, we investigated time–frequency dynamic functional connectivity among 11 brain regions of the default mode network by first projecting the coherence into the time and frequency domains, and subsequently by identifying clusters in the time–frequency domain using k-means clustering. Experiments on 14 temporal lobe epilepsy (TLE) patients and 21 age and sex-matched healthy controls were performed. The results show that functional connections in the brain regions of the hippocampal formation, parahippocampal gyrus, and retrosplenial cortex (Rsp) were reduced in the TLE group. However, the connections in the brain regions of the posterior inferior parietal lobule, ventral medial prefrontal cortex, and the core subsystem could hardly be detected in TLE patients. The findings not only demonstrate the feasibility of utilizing HHT in dynamic functional connectivity for epilepsy research, but also indicate that TLE may cause damage to memory functions, disorders of processing self-related tasks, and impairment of constructing a mental scene.

**Keywords** Dynamic functional connectivity · Time–frequency domain · Hilbert-Huang Transform · Default mode network · Temporal lobe epilepsy

---

Handling Editor: Louis Lemieux.

---

Ye Yuan and Ying Duan Co-first author.

---

✉ Chunlan Yang  
clyang@bjut.edu.cn

<sup>1</sup> Faculty of Environment and Life Sciences, Beijing University of Technology, Beijing, China

<sup>2</sup> Department of Bioengineering, Imperial College London, London, UK

<sup>3</sup> Beijing Universal Medical Imaging Diagnostic Center, Beijing, China

<sup>4</sup> School of Computer Science and Engineering, Beijing Technology and Business University, Beijing, China

<sup>5</sup> Beijing Tian Tan Hospital, Capital Medical University, Beijing, China

## Introduction

Epilepsy is a dysfunction caused by the abnormal discharge of brain neurons (Kramer and Cash 2012). At present, the understanding of epileptic seizures is still limited (Kramer and Cash 2012; Richardson 2012). In recent years, epilepsy has been regarded as a disorder of brain functional connectivity (Laufs 2012; Engel Jr et al. 2013; Stefan and Lopes Da Silva 2013; Caeyenberghs et al. 2015). Resting-state functional connectivity (rs-FC), constructed via functional magnetic resonance imaging (fMRI), has become an essential tool for exploring brain functions (Raichle et al. 2001; Damoiseaux et al. 2006; De Luca et al. 2006). In addition, it has been applied in temporal lobe epilepsy (TLE) patients (Liao et al. 2010; Vlooswijk et al. 2010, 2011; Zhang et al. 2011).

One of the well-applied approaches for constructing rs-FC is by using the temporal correlation, which links two brain

regions based on the mathematical similarity of regional signals (Fox et al. 2005; Fransson and Marrelec 2008; Lowe 2010; van den Heuvel et al. 2010). The independent analysis method (ICA) is another popular way of identifying spatially distinct regions with synchronized brain activity (De Luca et al. 2006; Calhoun et al. 2009). Other approaches for building rs-FC include coherence and partial coherence analysis (Salvador et al. 2005), phase relationships (Sun et al. 2005), clustering (Cordes et al. 2002; Mezer et al. 2009), and graph theory (Achard et al. 2006; Dosenbach et al. 2007).

Aside from the above-mentioned methods, dynamic functional connectivity has recently become a popular tool for researching brain functions. Previous studies have demonstrated that brain functions in a time-variant fashion, such as inter-regional correlations, can be affected by cognitive processes that occur on time scales of a typical scan (Esposito et al. 2006; Fransson 2006). The resting state contains different levels of attention, mind-wandering, and arousal. Hence, it can be inferred that rs-FC may undergo substantial changes across the duration of a scan.

The present study tries to investigate the abnormal dynamic rs-FCs of TLE compared with healthy controls (HCs). One challenge lies in obtaining the dynamic time–frequency characteristics of fMRI signals. In previous research, the time–frequency representations of fMRI time series were typically measured by implementing short-time Fourier transform (Mezer et al. 2009) or wavelet transform (Bullmore et al. 2001; Shimizu et al. 2004), which perform based on the assumption of the existence of the linearity or stationarity of input signals (Huang et al. 1998). Nevertheless, the blood-oxygen-level-dependent (BOLD) time series from the brain may not meet these expectations (Lange and Zeger 1997). Additionally, because of the constraint of the Uncertainty Principle (Robertson 1929), the majority of the widely-used time–frequency methods are restricted to providing high temporal and frequency resolution simultaneously. Hilbert-Huang transform (HHT) is a novel time–frequency method that capable of analyzing non-linear and non-stationary signals. Its application to electrophysiological studies has exhibited its efficacy in providing fine expressions of instantaneous frequency (Huang et al. 1998; Peng et al. 2005; Donnelly 2006). For instance, HHT has succeeded in being applied to electroencephalogram-based (EEG-based) seizure classification (Oweis and Abdulhay 2011), detection of spindles in sleep EEGs (Yang et al. 2007), and electrocardiogram de-noising (Tang et al. 2007). Yet, HHT has rarely been applied in fMRI studies.

In this study, we specifically focus on the differences in the default mode network (DMN) between TLE patients and HCs. So far, DMN has shown its importance in more complex brain functions more than a quiescent brain state

(Gusnard and Raichle 2001; Raichle et al. 2001). DMN is particularly useful for assessing internal mentation without external interactions (Buckner et al. 2008). For instance, some reports have revealed DMN's adaptive functions (Klinger and Cox 1987) while others emphasize the nature of DMN is to construct a mental scene (Hassabis and Maguire 2007). Moreover, DMN has also been found to play a part in self-referential or social processes (Schilbach et al. 2008; Mitchell 2009).

The specific functions of DMN have been the subjects of debates for decades. However, recent studies have shown that different anatomical structures account for distinct functions, and each component may work separately and together to achieve different goals (Andrews-Hanna et al. 2010). DMN consists of two distinct subsystems that converge on a midline core subsystem. The core subsystem (posterior cingulate [PCC] and anterior medial prefrontal cortex [aMPFC]) is active when people make self-related, affective decisions. In contrast, the medial temporal lobe subsystem (ventral MPFC [vMPFC], posterior inferior parietal lobule [pIPL], retrosplenial cortex [Rsp], parahippocampal cortex [PHC], and hippocampal formation [HF]) becomes engaged when decisions involve constructing a mental scene based on memory, while the dorsal subsystem (dorsal medial prefrontal cortex [dMPFC], temporoparietal junction [TPJ], lateral temporal cortex [LTC], and temporal pole [TempP]) is active when participants consider their present mental states.

To perform dynamic rs-FC analyses of DMN, a novel data-driven pipeline based on HHT was proposed. Firstly, the BOLD signal of 11 regions of DMN was extracted. Subsequently, each time series was processed by HHT to generate time–frequency representation. Afterwards, the coherence was performed across regions based on both time and frequency decomposed signals. Finally, the k-means clustering algorithm was used to extract the recurred rs-FCs among all the rs-FCs constructed at every time and frequency point for each subject. The differences between TLE patients and HCs were detected.

## Materials and Methods

### Participants

Thirty-five subjects were recruited for the rs-fMRI scanning, including 21 healthy volunteers recruited from Beijing University of Technology and 14 TLE patients recruited from Beijing Tiantan Hospital. Informed and written consent was obtained from each participant. All the participants are right-handed and age ranged from 18 to 40, with more than 6 years of education. MRI exclusion criteria included a history of psychiatric or neurological conditions, as

well as psychoactive medication use. Besides the criteria mentioned above, all patients were checked by MRI scanners showing no significant abnormalities of their brains, met the diagnostic criteria issued by the International Anti-Epilepsy Alliance (ILAE) and were diagnosed with typical TLE. In addition, the courses of all the TLE patients are more than 2 years, with no fewer than two episodes in a month. The statistical information of all the participants can be found in Table 1.

## MRI Acquisition

The fMRI data of all subjects were acquired using a 3T Siemens Trio scanner equipped with a 12-channel radiofrequency coil in the resting state.  $T_2^*$ -weighted functional images were acquired using a gradient-echo EPI sequence with TE = 30 ms, TR = 2.14 s, flip angle = 75°, slice thickness = 3.5 mm and gap = 1 mm, FOV = 220 × 220 mm<sup>2</sup>, matrix size = 64 × 64, time points = 240.

## Image Preprocessing

In the present study, functional images were preprocessed following a standard pipeline by the data processing software DPARSF (Yan et al. 2016). DICOM files were first converted to NIFTI files, then the first 10 functional volumes of each subject were removed to avoid potential disturbance caused by the non-equilibrium effects of magnetization. Subsequent processes were implemented on the remaining functional images, including slice timing correction, motion correction, and spatial normalization (Evans 1993). Specifically, data with translational and/or rotational motions exceeded  $\pm 2$  mm or  $\pm 2$  degree was excluded, and a standard EPI template in Montreal Neurological Institute (MNI) space was used for normalization. The data had been initially processed using the confound regressor derived from the cerebral spinal fluid (CSF) and white matter (WM) masks in REST ([www.restfmri.net](http://www.restfmri.net)), as well as Friston 24 head motion

parameters. The linear trend was then regressed out on each voxel to eliminate signal drifts caused by scanner instability or other factors. The signal of each voxel was normalized by subtracting the temporal mean and dividing by the temporal standard deviation. Bandpass filtering (0.01–0.08 Hz) was performed to obtain the low-frequency rs-fMRI oscillation signals. Finally, the time series of each region of interest (ROI) was extracted as the mean time courses of all voxels within the ROI for each subject and each of the 11 ROIs defined using the coordinates provided by (Andrews-Hanna et al. 2010), as shown in Table 2.

## Hilbert-Huang Transform

The time courses of the ROIs were the entry to HHT to ultimately obtain the instantaneous frequency. The HHT algorithm consists of two main processes. The intrinsic mode functions (IMFs) are firstly extracted from the input signal based on the empirical mode decomposition (EMD). Secondly, the Hilbert transform is used on each

**Table 2** The name, abbreviation, and partition of the 11 ROIs of DMN

Name	Abbreviation	Partition
Hippocampal formation	HF	VS
Parahippocampal gyrus	PHC	VS
Retrosplenial cortex	Rsp	VS
Posterior inferior parietal lobule	pIPL	VS
Ventral medial prefrontal cortex	vMPFC	VS
Posterior cingulate cortex	PCC	CS
Anterior MPFC	aMPFC	CS
Temporal pole	TempP	DS
Lateral temporal cortex	LTC	DS
Temporoparietal junction	TPJ	DS
Dorsal MPFC	dMPFC	DS

VS ventral subsystem, CS core subsystem, DS dorsal subsystem

**Table 1** Clinical information and IQ scores of TLE patients and healthy participants

Parameters	Mean $\pm$ SD		T	P
	TLE group (n = 14)	HC group (n = 21)		
Age (years)	27.179 $\pm$ 5.387 (18–37)	25.071 $\pm$ 2.352 (20–31)	1.303	0.164
Sex (males: females)	8:6	13:8	NA	0.613
Age of onset (years)	12.643 $\pm$ 7.045	NA	NA	NA
Course of TLE (years)	14.143 $\pm$ 5.153	NA	NA	NA
VIQ	88.286 $\pm$ 11.565	112.762 $\pm$ 10.440	−6.510	<0.001
PIQ	96.643 $\pm$ 9.589	112.286 $\pm$ 8.362	−5.114	<0.001
FIQ	91.500 $\pm$ 8.742	113.667 $\pm$ 7.971	−7.756	<0.001

SD standard deviation, HC healthy control, N number, VIQ verbal intelligence quotient, PIQ performance intelligence quotient, FIQ full-scale intelligence quotient

IMF to acquire the analytic transform to compute the instantaneous frequency. The details of each step are described as follows:

### (1) Empirical Mode Decomposition

The EMD algorithm (Huang et al. 1998) is to decompose an input signal into a finite set of generally simple oscillatory components, namely, the IMFs. In general, EMD breaks down the input signal  $s(t)$  into a set of  $IMF_i(t)$  and a monotonic residue signal  $r(t)$ :

$$s(t) = \sum_{i=1}^N IMF_i(t) + r(t) \quad (1)$$

where  $N$  is the number of IMFs. There are two requirements that each IMF must satisfy:

(I) Throughout the time course of the IMF, the number of local extrema and the number of zero-crossings must either be equal or differ at most by one;

(II) The mean value of the envelope outlined by the local maxima and the envelope outlined by the local minima is constantly zero.

To practically extract IMFs, an iterative algorithm known as the sifting process was applied:

Step 1: Identify all the local extrema of the input signal  $s(t)$ ;

Step 2: Connect all the local maxima by using a cubic spline line as the upper envelope  $e_u(t)$ , and repeat the procedure for all the local minima to generate the lower envelope  $e_l(t)$ ;

Step 3: Calculate the mean envelope  $e_m(t)$  from  $e_u(t)$  and  $e_l(t)$ ;

Step 4: Calculate the difference between the input signal and the mean envelop:  $r(t) = s(t) - e_m(t)$ ;

Step 5: If  $r(t)$  satisfies the above-mentioned two requirements of IMF, set  $IMF_i(t) = r(t)$ . Otherwise, set  $r(t)$  becomes the new  $s(t)$  and repeats the process from Step 1.

To obtain the remaining IMFs, the same procedure is performed repetitively to the residual  $r(t) = s(t) - IMF_i(t)$  until  $r(t)$  becomes a monotonic function.

### (2) Hilbert Transform

Hilbert Transform was implemented to compute the instantaneous frequency of each IMF. For a signal  $s(t)$ , its Hilbert Transform  $H[x(t)]$  is defined as:

$$H[s(t)] = \frac{P}{\pi} \int_{-\infty}^{+\infty} \frac{s(\tau)}{t - \tau} d\tau \quad (2)$$

where  $P$  is the Cauchy principal value (Surhone et al. 2013). Hilbert Transform derives the analytic representation of the input real-valued signal, which can be used to delineate the local properties of  $s(t)$  (Peng et al. 2005). The analytic transform  $z(t)$  of  $s(t)$  is defined as:

$$z(t) = s(t) + iH[s(t)] = a(t)e^{i\varphi(t)} \quad (3)$$

$$a(t) = \sqrt{s^2(t) + H^2[s(t)]} \quad (4)$$

$$\varphi(t) = \arctan\left(\frac{H[s(t)]}{s(t)}\right) \quad (5)$$

where  $a(t)$  is the instantaneous amplitude, and  $\varphi(t)$  is the instantaneous phase. Therefore, the instantaneous frequency is calculated as the time derivative:

$$\omega(t) = \frac{d\varphi(t)}{dt} \quad (6)$$

### Coherence Analysis

One measure of time series dependency in the time–frequency domain is the cross wavelet transform (XWT) (Grinsted et al. 2004), which is the element-wise conjugate multiplication between coefficients of each time series in the transformed domain (Eq. (7)).

$$W^{xy} = W^x \times W^y \quad (7)$$

where  $W^x$  and  $W^y$  are transformed signals  $x$  and  $y$ , and  $\times$  represents element-wise conjugate multiplication.

Modified by (Yaesoubi et al. 2015), the above measure is firstly normalized by signal spectral power. This step is introduced to ensure the estimation of coherence is biased toward neither part of the signal with more power. Moreover, the normalized measure is smoothed subsequently to avoid bias toward unity. This smoothing and normalization combined measure is called a wavelet coherence transform (WTC), which is defined as follows:

$$R = \frac{S(W^{xy})}{\sqrt{S'(|W^x|^2)}\sqrt{S'(|W^y|^2)}} \quad (8)$$

In the present study, we adopt the coherence computation into HHT.

### Clustering Analysis

To characterize the components of each subject at each time–frequency point, we have estimated the rs-FC of each subject at every time–frequency point. Furthermore, there is an assumption that some of the connectivity patterns may recur over time, which leads to the search for rs-FC patterns recurred in both time and frequency domains. To achieve this, estimated rs-FCs along the subject, time, and frequency were firstly concatenated (see Fig. 1), then a

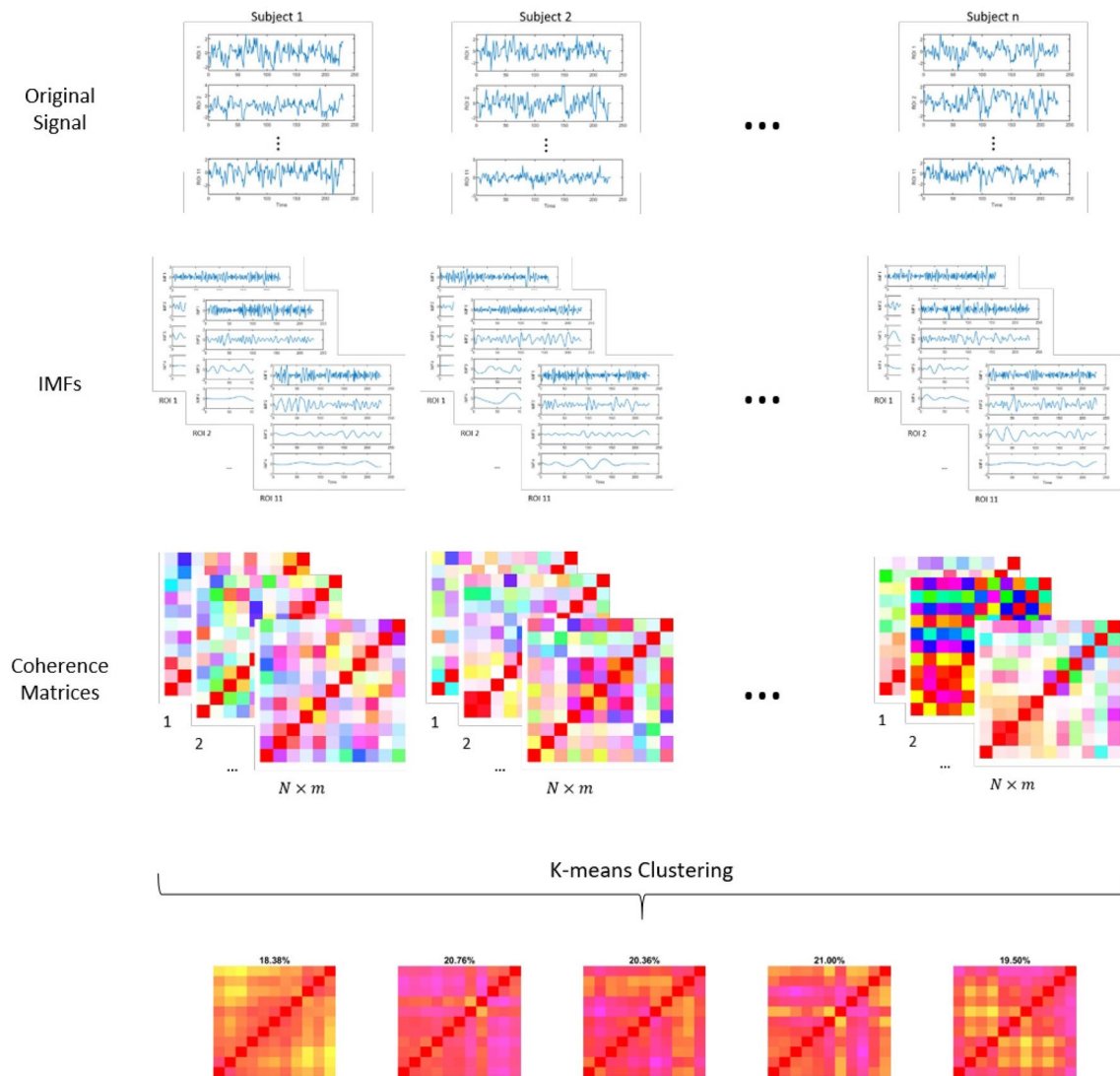


**Fig. 1** General flowchart of constructing the HHT-based dynamic rs-FC. The original signals (data size=number of subjects $\times$ number of ROIs $\times$ number of time points) were decomposed by the EMD algorithm into six IMFs (data size=number of subjects $\times$ number of ROIs $\times$ number of time points $\times$ number of IMFs), the Hilbert transform was then applied on the first three IMFs to generate the coherence matrices ( $N$  depicts the specific pair of ROIs,  $m$

indicates all the frequencies and time points) including information from the time and frequency domains. Finally, k-means clustering was performed to identify the most recurrent five states (data size=number of ROIs $\times$ number of ROIs). HHT Hilbert-Huang Transform, EMD empirical mode decomposition, IMF intrinsic mode function

k-means clustering algorithm was implemented to obtain a finite set of ' $k$ ' recurring rs-FCs.

The selection of an optimal ' $k$ ' in this study was referring to (Yaesoubi et al. 2015), which is based on the calculation of the F-ratio for each ' $k$ ' in the range of two to nine. Here, F-ratio is defined as the average ratio of the sum of the squared distance between each cluster point and the corresponding cluster centroids (inside cluster dispersion) to the sum of the square distance of the points outside of the cluster to the same estimated centroids (outside cluster dispersion).

Additionally, the initial random assignment of the point to randomly selected clusters in the clustering may bias the final results. Hence, 500 times of k-means were run on the same data with a random initial guess of clusters assignment, and the selection of the clustering result was based on the minimum sum of distances of each point to its corresponding cluster centroid.

## Traditional rs-FC Construction

To demonstrate the feasibility and validity of the proposed pipeline for dynamic FC analysis, traditional FC of HCs and TLE patients were also constructed using GREYNA (Wang et al. 2015). For each subject, the 11 ROIs within DMN were utilized to construct rs-FCs. Each ROI represents a node, the value of each node is replaced by the arithmetic mean of the BOLD signal within its corresponding ROIs.

The time series of each ROI were extracted, and an  $11 \times 11$  coherence matrix was obtained by calculating the Pearson correlation coefficients between-nodes to indicate the interactions between different ROIs. In addition, the coherence matrix of each subject is Fisher-z transformed to obtain a z-value matrix close to normal distribution to facilitate subsequent statistical analysis (Belliveau et al. 1991).

## Statistical Analysis

The unbalanced sample sizes in this study has a risk to bias the coherence analysis. To verify the validity of the present fMRI data, age and sex of our recruited subjects were analyzed statistically using SPSS 26.0. Shapiro–Wilk tests were conducted to examine the normality of age in HCs and TLEs. Further independent samples t-test was performed because the age in both group can satisfy a normal distribution. Meanwhile, chi-square test was performed to examine the significance of sex in both groups.

Dynamic rs-FC analysis has realized group-level qualitative comparisons. For further quantitative comparisons between groups, independent samples t-test was conducted based on the rs-FCs to detect the significance of the group-level differences (namely the significant abnormality of rs-FCs in TLE group) using GREYNA.

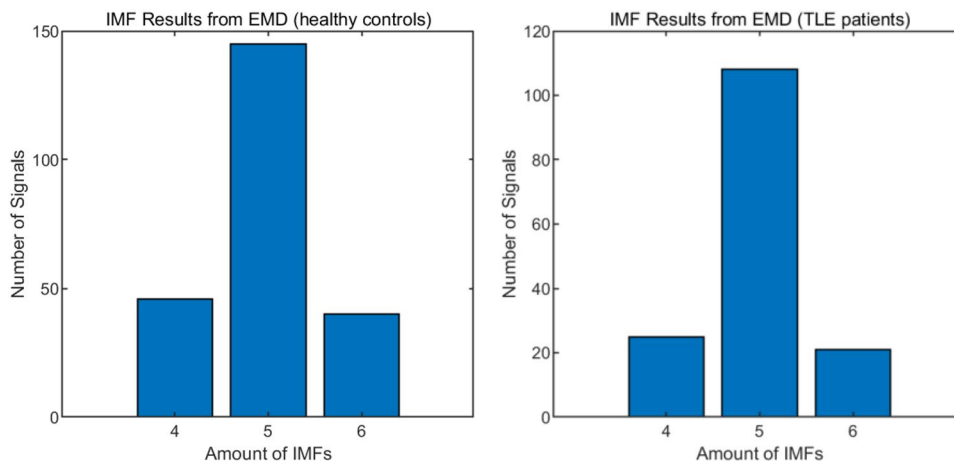
## Results

The rs-fMRI data of 21 HCs and 14 TLE patients were analyzed. Shapiro-Wilk tests were conducted on the age of HCs and TLEs and showed no significance in both groups (HC:  $p = 0.063$ ; TLE:  $p = 0.689$ ), indicating the age of both groups satisfy normal distributions. In addition, no significant difference was found in the age of HCs and TLEs (two-tailed independent samples  $t$  test;  $t_{(16,342)} = -1.379$ ;  $p = 0.187$ ), as well as sex of the two groups (two-sided chi-square test;  $p = 0.778$ ). No bias was produced due to the unbalanced sample sizes.

Owing to its intrinsic adaptivity, the EMD procedure generates a different number of IMFs for each time series. In the HC group, a total of 231 signals (number of subjects  $\times$  number of ROIs) passed through the EMD analysis. The HC group in Fig. 2 shows 145 out of 231 signals decomposed into five IMFs, while four IMFs were obtained from 46 signals and six IMFs were extracted from 40 signals. Similarly, 154 signals passed through the EMD analysis in the TLE group, of which 108 signals decomposed into five IMFs, while four IMFs were obtained from 25 signals and six IMFs were extracted from 21 signals.

By additionally calculating the Pearson correlation between each IMF and the corresponding original signal, we found that the first three IMFs exhibited relative similarity to the original signal (Fig. 3). The respective median of the first three IMFs in the HC group was 0.778, 0.616, and 0.160, whereas the median of the last three IMFs was 0.0057, 0.0081, 0.0156, respectively. Similar to the results of HCs, the results of Pearson correlation in the TLE group are 0.779, 0.621, 0.149, 0.0077, 0.0056, -0.0012. Moreover, the quantity of IMFs should be equal among ROIs in the following computation of coherence matrices. Hence, the first three IMFs were selected as the entry point for the subsequent processes.

**Fig. 2** The distribution of IMF numbers after EMD analysis (in a range of 0 to 150 with steps equal to 50 in the HC group and 0 to 120 with steps equal to 50 in the TLE group). IMF intrinsic mode function, EMD empirical mode decomposition



The number of clusters should be determined before performing k-means clustering. Referring to the previous research of reference (Yaesoubi et al. 2015), the value from 2 to 9 for ‘k’ was trialed. From Fig. 4, the larger the ‘k’ value, the smaller the F-Ratio. Considering the calculation complexity, the value of 5 for ‘k’ is on the elbow of the

F-ratio curve that meets the expectation of minimum inside cluster dispersion while maximum outside cluster dispersion. Henceforth, the recurring coherence matrices were finally summarized into five representative states.

For each state, the connections across the ROIs exhibited relatively strong coherence (Fig. 5). The median of

**Fig. 3** The Pearson correlation between each IMF and the corresponding original signal (in a range of -0.2 to 1 with steps equal to 0.2 in both groups). IMF, intrinsic mode function

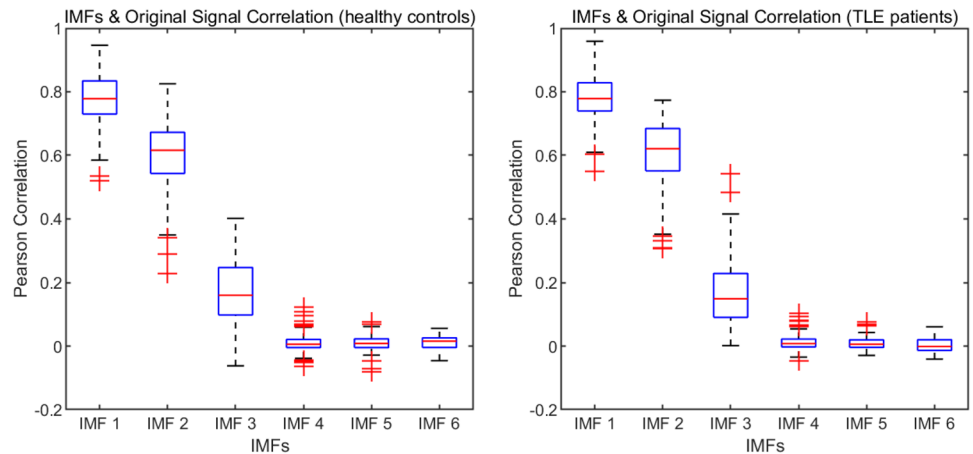


**Fig. 4** F-ratio of each trial with an increased number of clusters (in a range of 0 to 1 with steps equal to 0.2 in both groups)

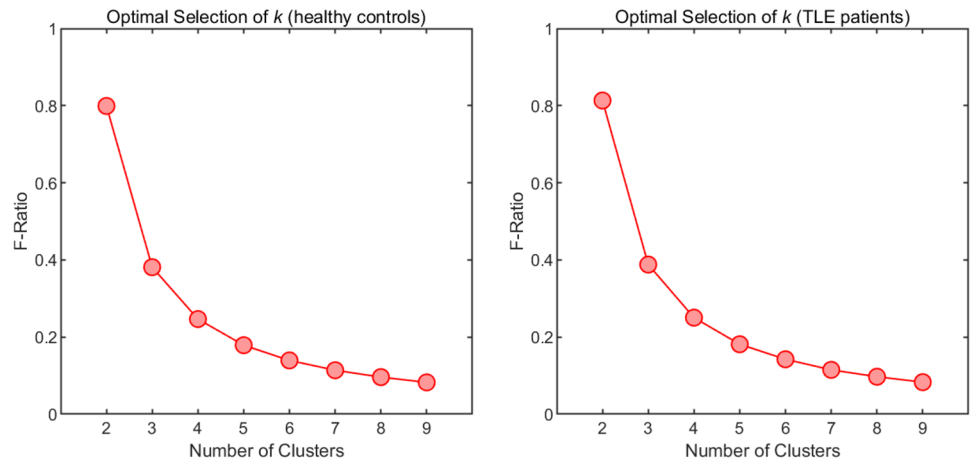


**Fig. 5** The coherence strength in each state (in a range of 0.84–0.89 with steps equal to 0.005 in the HC group and 0.835–0.89 with steps equal to 0.005 in the TLE group)

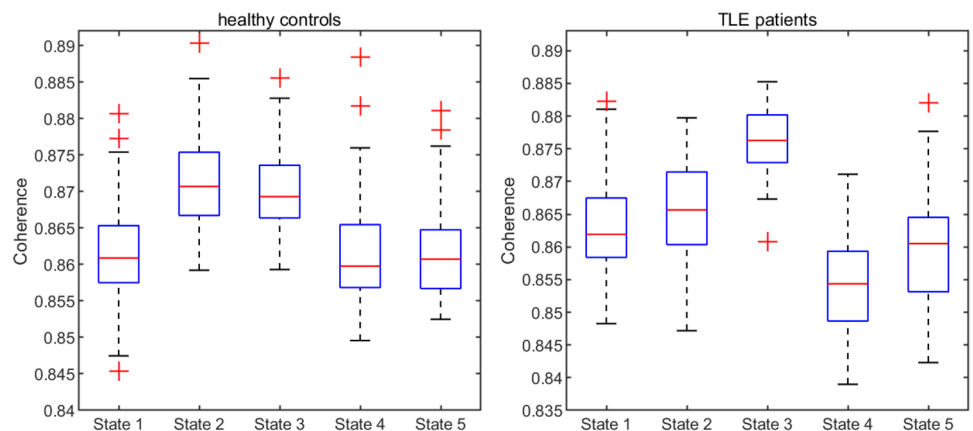
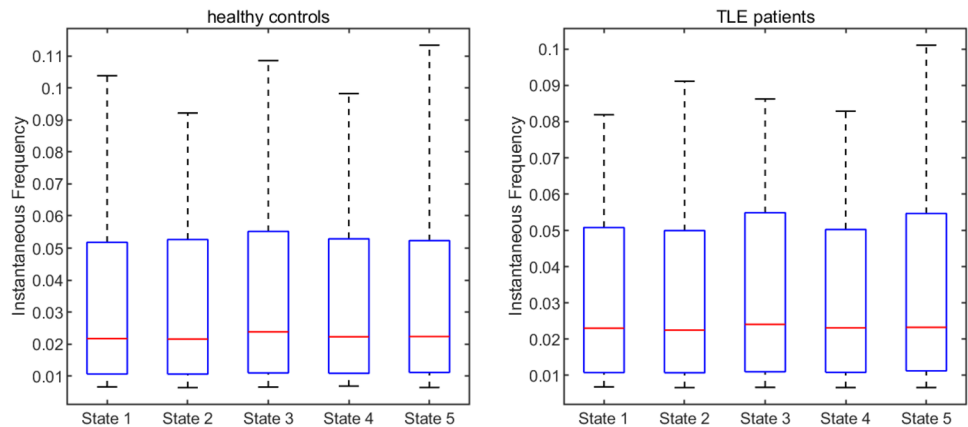


**Fig. 6** The distribution of instantaneous frequency in each state (in a range of 0–0.11 with steps equal to 0.01 in the HC group and 0–0.1 with steps equal to 0.01 in the TLE group)



coherence for each state in the HC group was 0.873, 0.866, 0.862, 0.857 and 0.866, respectively, which was consistent with the selection of the ROIs that all emanate from the DMN. Similarly, the median of coherence for each state in the TLE group was 0.853, 0.860, 0.875, 0.861, 0.870.

Moreover, the instantaneous frequency of each state is similarly distributed (Fig. 6), and they are all centered in the low-frequency band (0.02–0.03 Hz), which accords with the resting state of scanned functional images.

We present the states as the cluster centroids in Fig. 7 based on the estimated recurring functional coherence matrices. Since the matrices are all complex valued, we exploit intensities to illustrate the coherence extent, and colors to demonstrate the phase information. We added a polar diagram to show the corresponding color of phase-lagging and used a polar scatter diagram to exhibit the distribution of phases lagging across all component pairs. Moreover, a positive phase in the upper triangular of each coherence matrix in Fig. 7 shows that the time course on the horizontal axis is lagging with respect to the one on the vertical axis.

Note that the coherence across regions for all the states is relatively high and similar (Fig. 5), and the ROIs of DMN selected have adjacent anatomical structures, so their connection is strong. In Fig. 7, the coherence intensity is close to the same phase, that is, the red area in the graph. Because the coherence between each ROI is strong and the color difference is not obvious, the region segmentation is carried out in Fig. 7 later, and the segmented regions are numbered to depict the results clearly and readily.

Notably, state-1 in Fig. 7A exhibits three adjacent regions of the ventral subsystem (i.e., HF, PHC, and Rsp), as marked in area-①. Similarly, the subdivision area of the ventral subsystem is also detected in area-① of state-3.

For the state-4 shown in Fig. 7A, both the ventral subsystem (area-①) and the core subsystem (area-②) show a strong positive correlation (phase-lag  $\sim 0$ ), and state-5 shows three subsystems, including the dorsal and

ventral-core combined subsystems. For state-3, there is a similar regional distribution as in state-1, that is, the HF-PHC-Rsp subdivision, while the connections outside the areas present the opposite phase-lag. In addition, the entire core and dorsal subsystems, plus pIPL and vMPFC from the ventral subsystem can also be detected in its area-② of state-3. For state-2, the distribution state of the internal network is random, which can be regarded as the residual error of the other four states.

Similar to the HC group, the subdivision within the ventral subsystem including HF, PHC and Rsp is also found in both state-3 and state-5 of the TLE group (Fig. 7B). In the area-② of state-3 in the TLE group, the coherence of the entire core and dorsal subsystem, as well as part of the ventral subsystem region is stronger than HCs. In addition, from area-② of state-5 (Fig. 7B), the part of the inner dorsal subsystem shows an obvious positive correlation. However, in the TLE group, the distribution of the internal network of other states is relatively ambiguous. Therefore, we can conclude that TLE patients retain parts of the functions in DMN, but more irregular connections appeared among the selected ROIs compared to HCs. In general, the probability of occurrence of the five states in both groups is relatively average, all around 20%.

As shown in Table 3, significant differences between the nodes of HCs and TLEs were detected (two-tailed independent samples *t* test), including HF-PHC, PHC-Rsp, Rsp-dMPFC, and pIPL-TempP.

## Discussion

### Advantages and Limitations

In this work, we investigated the time–frequency dynamics of rs-FC among 11 brain regions of DMN by exploiting the data of HCs and TLE patients. First, the BOLD signal of 11 regions of DMN was extracted to the time series signals,



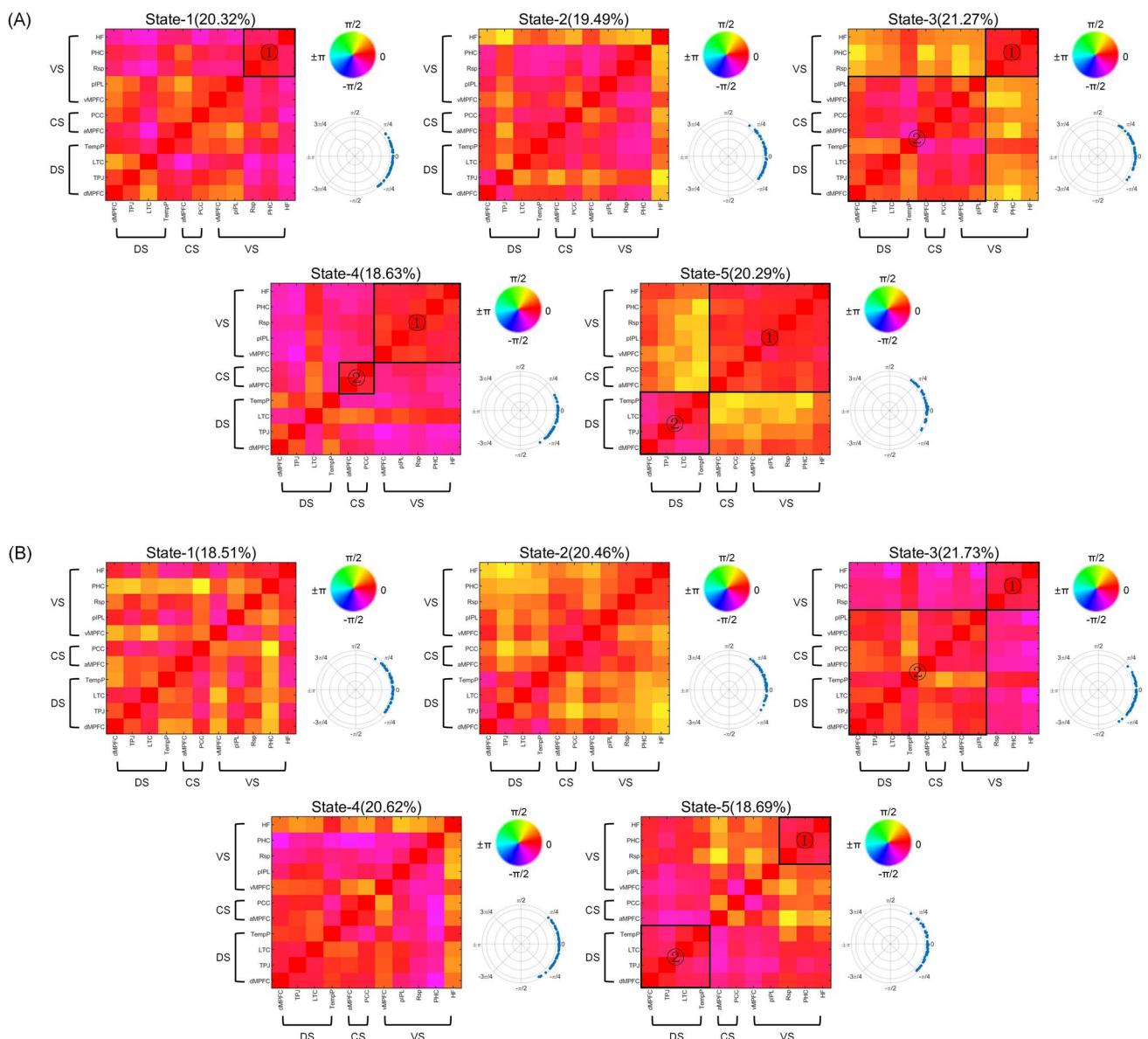


**Fig. 7** Recurrent states of connectivity estimated as the cluster centroids formed in the time–frequency domain: **A** HC group **B** TLE group. For each pattern, intensity denotes coherence strength, phase information is presented as the color map and scatter plots

**Table 3** The abnormal functional connections (nodes) caused by TLE

Number	ROI 1	ROI 2	<i>p</i> value	<i>t</i> value
1	HF	PHC	0.048	2.06
2	PHC	Rsp	0.016	2.54
3	Rsp	dMPFC	0.013	2.64
4	pIPL	TempP	0.047	2.06

ROI Region of Interest, HF hippocampal formation, PHC parahippocampal gyrus, Rsp retrosplenial cortex, pIPL posterior inferior parietal lobule, dMPFC dorsal medial prefrontal cortex, TempP temporal pole

which were then decomposed by the EMD algorithm into IMFs. Afterwards, the coherence of IMFs was projected into the time domain and frequency domain respectively using WTC, and subsequently the clusters in which coherence forms in the time–frequency domain were identified by the k-means clustering algorithm.

In the present study, HHT was introduced to construct dynamic rs-FCs of rs-fMRI. The advantage of using HHT here is mainly its effectiveness on the characters of the fMRI data. Previous research has firstly shown that the BOLD-fMRI data may not strictly follow the assumptions of linearity and stationarity (Lange and Zeger 1997). Owing to the adaptivity of the EMD algorithm, HHT

can be used to process BOLD (non-linear and non-stationary) signals directly when compared with previous time–frequency analysis methods (such as WTC and short-time Fourier transform). Limited by the Uncertainty Principle, previous time–frequency-based methods cannot achieve high temporal and frequency resolution simultaneously (Robertson 1929). While many previous studies have reported that HHT does not suffer from the above-mentioned trade-off (Huang et al. 1998; Peng et al. 2005; Donnelly 2006) and thus may be an appropriate candidate for characterizing fMRI signals with the time–frequency representation. Our results exhibited that HHT can be used to describe fMRI signals in both high temporal and frequency resolution (as shown in Fig. 7).

Chang and Glover (2010) showed that the nature of coherence between the default mode network (DMN) and the task-positive network (TPN) is temporally dynamic, but not frequency-dependent. Accordingly, we have observed the comparable distributions of instantaneous frequency in each state, while vastly differing connection patterns were revealed in Figs. 6 and 7. Moreover, introducing the complex value enabled us to observe lagged coherence between input signals over the full range, from complete in-phase (0) coherence to complete out-of-phase ( $\pm\pi$ ). Hence, the differences in clustering results are reflected in various connectivity patterns, and the input signals that change in various phases also play an essential role in showing the specific strength of coherence. Conventional measures of correlation such as the Pearson correlation are unable to provide phase-lagged coherence, as demonstrated by the comparisons between conventional rs-FC construction approach and our proposed HHT-based dynamic rs-FC construction approach. Specifically, conventional approaches typically generate the coherence matrix by calculating the Pearson correlation coefficients between-nodes, while the novel dynamic approach can provide lagged phase information using a polar diagram and polar scatter diagram (Fig. 7).

The dynamic rs-FC in the present study revealed the complex connection patterns within DMN. Particularly in the HC group (Fig. 7A), the coherence of at least two subsystems is relatively strong in state-3, state-4, state-5 (as shown in Fig. 7A), of which a strong coherence in the core subsystem can be detected in terms of the specific connection patterns and input signals, compared with the other two distinct subsystems. This is consistent with the finding that the core subsystem is a link between two subsystems, and exhibits high levels of distributed functional connectivity throughout the cortex (Hagmann et al. 2008; Buckner et al. 2009). Additionally, in state-3 of the HC group (Fig. 7A), the core subsystem showed a higher correlation with the dorsal subsystem than with the ventral one. Previous studies show that the possible neural overlap

of the dorsal subsystem among affective, self-referential, and social cognitive processes suggests a broader role for this subsystem (Frith and Frith 2003; Ochsner et al. 2004; Olsson and Ochsner 2008; Mitchell 2009), which may lead to a stronger correlation between the dorsal and core subsystems. Conventional rs-FC analysis approaches can only construct the brain network in one time point, while the present dynamic rs-FC analysis technique makes it possible to investigate the dynamic characteristics of rs-FC over time, which is able to capture more detailed abnormal nodes that are hard to be detected using conventional approaches. Previous research for rs-FC analysis assumed that the functional network connectivity is stable, but there are growing evidence that rs-FC is dynamic, time-dependent, and related to ongoing rhythmic activities (Allen et al. 2014; Liu et al. 2018), investigating the dynamic characteristics of rs-FC over time may better reveal the fundamental properties of brain networks (Calhoun et al. 2014; Gratton et al. 2018), which is in line with our results.

When it comes to the interpretability of results, this study implicates a certain degree of ambiguity. Although we observed five states of DMN, it is difficult to identify the relationships of the states to their corresponding behavioral functions because the specific procedure of k-means clustering is difficult to be figured out. Moreover, it is also crucial to determine if there is an order of emerging states, and if so, what that might consist of. Another limitation lies in terms of our choice of the clustering algorithm. In the present study, we selected the k-means clustering algorithm. However, it is a well-used method that searches clusters with convex boundaries. Recent studies have also taken advantage of linear decomposition to explore functional connectivity (Schilbach et al. 2008; Leonardi et al. 2013). Meanwhile, EMD has its limitations, as evidenced through the end effect and model mixing problem (Huang et al. 1998). Improved EMD methods have come to light recently, which could be employed in further research. We hope to compare the existed methods in our future studies, to gain more insights on dynamic rs-FC.

In terms of the applications of HHT, we subsequently investigated the abnormality of TLE patients against HCs by HHT-based dynamic functional connectivity.

### Differences in the DMN of TLE Patients Against HCs

In this study, we tried to investigate the differences between HCs and TLE patients by comparing the time–frequency dynamics of rs-FC among 11 brain regions of DMN between the two groups. Based on the previous studies on TLE patients, Allone et al. (2017) found that TLE may lead to impairment of cognitive functions such as memory and attention, and language disorders. Accordingly, the results show that compared with HCs, more random functional

network connections were found in the TLE group (as shown in Fig. 7B). Thus, the active regions in the DMN of TLE patients exhibit a significant reduction (i.e., the cognitive functions of TLE patients are less than HCs), which depicts that TLE may lead to impairment of brain functions.

Notably, this study found that the connections among pIPL, vMPFC, and the core subsystem in the TLE group are comparatively less. Simultaneously, a significant difference in the node of pIPL-TempP ( $p < 0.05$ ;  $t = 2.06$ ) was detected using two-tailed independent samples  $t$  test. Based on the previous studies of cognitive science, neuroscience, and clinical psychology, Andrews-Hanna et al. (2014) found that pIPL is the intersection of auditory, visual, and somatosensory information and attention. When interacting with the medial temporal subsystem, vMPFC may affect the association and construction of mental simulation (Andrews-Hanna et al. 2014). Furthermore, studies suggest that the core subsystem (i.e., PCC, aMPFC) is active when people make self-relevant, affective decisions (Andrews-Hanna et al. 2010). Specifically, PCC can be subdivided into ventral and dorsal components (Spreng et al. 2009; Andrews-Hanna 2012; Leech et al. 2012), in which the ventral PCC plays a broad role in nearly all self-related tasks, including tasks of self-referential processing, episodic memory, future thinking, spatial navigation, and conceptual processing (Vogt et al. 2006; Binder et al. 2009; Leech et al. 2011; Qin and Northoff 2011). The dorsal PCC is highly relevant to autonomic arousal and awareness (Baars et al. 2003; Brewer et al. 2013) and environmental changes (Leech and Sharp 2014). Meanwhile, aMPFC is activated when people search for personal knowledge, consider their future objectives or mental states, simulate future events or social interactions, and make decisions associating with the people they value (e.g., their friends or relatives) (Benoit et al. 2010; Krienen et al. 2010; Pearson et al. 2011; Denny et al. 2012; Murray et al. 2012; Moran et al. 2013). With the exception of positive emotional material, aMPFC is also linked to negative emotional material, particularly for such materials regarded with high personal significance (e.g., when one predicts physical pain (Ochsner et al. 2006; Atlas et al. 2010)).

Additionally, in most of the ventral subsystems of HCs (Fig. 7A), HF, PHC, and Rsp are closely related to other brain regions of DMN and are obviously activated during the process of memory. Compared with HCs, the HF-PHC-Rsp subdivision in the TLE group is more difficult to be detected (Fig. 7B). Meanwhile, significant differences were found in the nodes of HF-PHC ( $p < 0.05$ ;  $t = 2.06$ ), PHC-Rsp ( $p < 0.05$ ;  $t = 2.54$ ), and Rsp-dMPFC ( $p < 0.05$ ;  $t = 2.64$ ). Due to the random connections in the DMN of TLE patients, the memory functions of TLE patients may be damaged to some degree. Furthermore, previous studies have shown that the abnormal discharge of TLE can interrupt connections within

DMN (Coan et al. 2014), which is consistent with the results of our study. Moreover, Pittau et al. (2012) found that the connection strength between the hippocampus and DMN of TLE patients decreased evidently, which may present the neural mechanism of cognition deficits in TLE patients. Hence, mental disorders are related to the functional impairment of DMN.

The epileptic seizures are also related to hippocampal sclerosis (HS), in which the changes of rs-FCs are obvious. Stretton et al. (2013) investigated the memory tasks of unilateral TLE patients with HS, the results exhibit a significant reduction in the strength of patients' rs-FCs. The stronger the abnormal connections are, the worse the completion of memory tasks is. In the five states of TLE patients (Fig. 7B), the connections between HF and other regions are obviously less than HCs, which suggests that the changes of rs-FCs may probably predict the corresponding clinical symptoms.

Although we detected the abnormal connections in the DMN of TLE patients, the experiments are constrained by the sample size. In our future work, more data would be acquired to determine the specific epilepsy subtypes and obtain more pathological mechanisms accurately. In terms of the image preprocessing pipeline, our criteria and thresholds for translational and/or rotational motions exclusion are outdated, future work can optimize the quantification and control of subject motions using more advanced methods, such as Framewise displacement (FD), derivative variance (DVAR), and convolutional neural network guided retrospective motion correction approaches (Haskell et al. 2019).

Furthermore, it may be feasible to apply the pipeline of HHT-based dynamic rs-FCs to other mental diseases. Meanwhile, our study mainly investigated the 11 regions within DMN, future studies can explore other ROIs that are essential for cognitive functions. Hence, with the increase of research on TLE, it will be more used in diagnosis and treatment in the future to perform the diagnosis more accurately.

## Conclusions

In the present work, we proposed a pipeline to construct time–frequency dynamic rs-FCs based on rs-fMRI data by a data-driven approach HHT and explored its application in TLE. By investigating the subsystems of DMN, 11 regions within DMN were selected as ROIs and subsequently the dynamic aspect of corresponding subject-specific functional network connectivity in both time and frequency domains were examined. Finally, the dynamic coherence of time courses was summarized with a finite number of

recurring patterns of connectivity estimated by k-means clustering of the complex-valued rs-FCs. Distinctions and connections among three subsystems of DMN were observed through recurring connectivity patterns in the time–frequency domain. The results of group-level analyses depict that TLE may cause damage to memory functions, disorders of processing self-related tasks, and impairment of constructing a mental scene. Overall, the findings demonstrate the feasibility of utilizing HHT in dynamic functional connectivity for epilepsy research, which may provide a basis for the diagnosis and evaluation of TLE.

**Supplementary Information** The online version contains supplementary material available at <https://doi.org/10.1007/s10548-023-00966-9>.

**Acknowledgements** Thanks for the support from Intelligent Physiological Measurement and Clinical Translation, Beijing International Base for Scientific and Technological Cooperation.

**Authors contribution** YY: Conceptualization, Methodology, Software, Validation, Formal analysis, Investigation, Writing—original draft, Writing—review and editing, Visualization. YD: Resources, Data curation, Interpretation. WL: Conceptualization, Methodology, Software, Validation, Writing—original draft, Visualization. JR: Resources, Data curation. ZL: Resources, Data curation. CY: Conceptualization, Methodology, Software, Resources, Data curation, Writing—review and editing, Visualization, Supervision, Project administration, Funding acquisition.

**Funding** This study was supported by project grants from the Beijing Nova Program (xx2016120), National Natural Science Foundation of China (81101107, 31640035, 81601126), Natural Science Foundation of Beijing (4162008) and program for Scientific Research Project of Beijing Educational Committee (SQKM201710005013).

**Data Availability** The data that support the findings of this study are available from the corresponding author upon reasonable request.

## Declarations

**Conflict of interest** The authors have no relevant financial or non-financial interests to disclose.

## References

Achard S, Salvador R, Whitcher B et al (2006) A resilient, low-frequency, small-world human brain functional network with highly connected association cortical hubs. *J Neurosci* 26:63–72. <https://doi.org/10.1523/JNEUROSCI.3874-05.2006>

Allen EA, Damaraju E, Plis SM et al (2014) Tracking whole-brain connectivity dynamics in the resting state. *Cereb Cortex* 24:663–676. <https://doi.org/10.1093/cercor/bhs352>

Allone C, Buono VL, Corallo F et al (2017) Neuroimaging and cognitive functions in temporal lobe epilepsy: a review of the literature. *J Neurol Sci* 381:7–15. <https://doi.org/10.1016/j.jns.2017.08.007>

Andrews-Hanna JR (2012) The brain's default network and its adaptive role in internal mentation. *Neuroscientist* 18:251–270. <https://doi.org/10.1177/1073858411403316>

Andrews-Hanna JR, Reidler JS, Sepulcre J et al (2010) Functional-anatomic fractionation of the brain's default network. *Neuron* 65:550–562. <https://doi.org/10.1016/j.neuron.2010.02.005>

Andrews-Hanna JR, Smallwood J, Spreng RN (2014) The default network and self-generated thought: component processes, dynamic control, and clinical relevance. *Ann N Y Acad Sci* 1316:29–52. <https://doi.org/10.1111/nyas.12360>

Atlas LY, Bolger N, Lindquist MA, Wager TD (2010) Brain mediators of predictive cue effects on perceived pain. *J Neurosci* 30:12964–12977. <https://doi.org/10.1523/JNEUROSCI.0057-10.2010>

Baars BJ, Ramsøy TZ, Laureys S (2003) Brain, conscious experience and the observing self. *Trends Neurosci* 26:671–675. <https://doi.org/10.1016/j.tins.2003.09.015>

Belliveau JW, Kennedy DN, McKinstry RC et al (1991) Functional mapping of the human visual cortex by magnetic resonance imaging. *Science* 254:716–719. [https://doi.org/10.1016/S1076-6332\(03\)80199-X](https://doi.org/10.1016/S1076-6332(03)80199-X)

Benoit RG, Gilbert SJ, Volle E, Burgess PW (2010) When I think about me and simulate you: medial rostral prefrontal cortex and self-referential processes. *Neuroimage* 50:1340–1349. <https://doi.org/10.1016/j.neuroimage.2009.12.091>

Binder JR, Desai RH, Graves WW, Conant LL (2009) Where is the semantic system? A critical review and meta-analysis of 120 functional neuroimaging studies. *Cereb Cortex* 19:2767–2796. <https://doi.org/10.1093/cercor/bhp055>

Brewer J, Garrison K, Whitfield-Gabrieli S (2013) What about the “self” is processed in the posterior cingulate cortex? *Front Hum Neurosci* 7:647. <https://doi.org/10.3389/fnhum.2013.00647>

Buckner RL, Andrews-Hanna JR, Schacter DL (2008) The brain's default network: anatomy, function, and relevance to disease. *Ann NY Acad Sci* 1124:1–38. <https://doi.org/10.1196/annals.1440.011>

Buckner RL, Sepulcre J, Talukdar T et al (2009) Cortical hubs revealed by intrinsic functional connectivity: mapping, assessment of stability, and relation to Alzheimer's disease. *J Neurosci* 29:1860–1873. <https://doi.org/10.1523/JNEUROSCI.5062-08.2009>

Bullmore E, Long C, Suckling J et al (2001) Colored noise and computational inference in neurophysiological (fMRI) time series analysis: resampling methods in time and wavelet domains. *Hum Brain Mapp* 12:61–78. [https://doi.org/10.1002/1097-0193\(200102\)12:2%3c61::AID-HBM1004%3e3.0.CO;2-W](https://doi.org/10.1002/1097-0193(200102)12:2%3c61::AID-HBM1004%3e3.0.CO;2-W)

Caeyenberghs K, Powell HWR, Thomas RH et al (2015) Hyperconnectivity in juvenile myoclonic epilepsy: a network analysis. *NeuroImage Clin* 7:98–104. <https://doi.org/10.1016/j.nicl.2014.11.018>

Calhoun VD, Liu J, Adalı T (2009) A review of group ICA for fMRI data and ICA for joint inference of imaging, genetic, and ERP data. *Neuroimage* 45:S163–S172. <https://doi.org/10.1016/j.neuroimage.2008.10.057>

Calhoun VD, Miller R, Pearlson G, Adalı T (2014) The chronnectome: time-varying connectivity networks as the next frontier in fMRI data discovery. *Neuron* 84:262–274. <https://doi.org/10.1016/j.neuron.2014.10.015>

Chang C, Glover GH (2010) Time–frequency dynamics of resting-state brain connectivity measured with fMRI. *Neuroimage* 50:81–98. <https://doi.org/10.1016/j.neuroimage.2009.12.011>

Coan AC, Campos BM, Beltramini GC et al (2014) Distinct functional and structural MRI abnormalities in mesial temporal lobe epilepsy with and without hippocampal sclerosis. *Epilepsia* 55:1187–1196. <https://doi.org/10.1111/epi.12670>

Cordes D, Haughton V, Carew JD et al (2002) Hierarchical clustering to measure connectivity in fMRI resting-state data. *Magn Reson Imaging* 20:305–317. [https://doi.org/10.1016/S0730-725X\(02\)00503-9](https://doi.org/10.1016/S0730-725X(02)00503-9)

- Damoiseaux JS, Rombouts S, Barkhof F et al (2006) Consistent resting-state networks across healthy subjects. *Proc Natl Acad Sci* 103:13848–13853. <https://doi.org/10.1073/pnas.0601417103>
- De Luca M, Beckmann CF, De Stefano N et al (2006) fMRI resting state networks define distinct modes of long-distance interactions in the human brain. *Neuroimage* 29:1359–1367. <https://doi.org/10.1016/j.neuroimage.2005.08.035>
- Denny BT, Kober H, Wager TD, Ochsner KN (2012) A meta-analysis of functional neuroimaging studies of self-and other judgments reveals a spatial gradient for mentalizing in medial prefrontal cortex. *J Cogn Neurosci* 24:1742–1752. [https://doi.org/10.1162/jocn\\_a\\_00233](https://doi.org/10.1162/jocn_a_00233)
- Donnelly D (2006) The fast Fourier and Hilbert-Huang transforms: a comparison. *Proceedings of the multiconference on computational engineering in systems applications*, pp 84–88
- Dosenbach NU, Fair DA, Miezin FM et al (2007) Distinct brain networks for adaptive and stable task control in humans. *Proc Natl Acad Sci* 104:11073–11078. <https://doi.org/10.1073/pnas.0704320104>
- Engel J Jr, Thompson PM, Stern JM et al (2013) Connectomics and epilepsy. *Curr Opin Neurol* 26:186. <https://doi.org/10.1097/WCO.0b013e32835ee5b8>
- Esposito F, Bertolino A, Scarabino T et al (2006) Independent component model of the default-mode brain function: assessing the impact of active thinking. *Brain Res Bull* 70:263–269. <https://doi.org/10.1016/j.brainresbull.2006.06.012>
- Evans JSB (1993) The mental model theory of conditional reasoning: critical appraisal and revision. *Cognition* 48:1–20. [https://doi.org/10.1016/0010-0277\(93\)90056-2](https://doi.org/10.1016/0010-0277(93)90056-2)
- Fox MD, Snyder AZ, Vincent JL et al (2005) The human brain is intrinsically organized into dynamic, anticorrelated functional networks. *Proc Natl Acad Sci* 102:9673–9678. <https://doi.org/10.1073/pnas.0504136102>
- Fransson P (2006) How default is the default mode of brain function?: further evidence from intrinsic BOLD signal fluctuations. *Neuropsychologia* 44:2836–2845. <https://doi.org/10.1016/j.neuropsychologia.2006.06.017>
- Fransson P, Marrelec G (2008) The precuneus/posterior cingulate cortex plays a pivotal role in the default mode network: evidence from a partial correlation network analysis. *Neuroimage* 42:1178–1184. <https://doi.org/10.1016/j.neuroimage.2008.05.059>
- Frith U, Frith CD (2003) Development and neurophysiology of mentalizing. *Philos Trans R Soc Lond B* 358:459–473. <https://doi.org/10.1098/rstb.2002.1218>
- Gratton G, Cooper P, Fabiani M et al (2018) Dynamics of cognitive control: Theoretical bases, paradigms, and a view for the future. *Psychophysiology*. <https://doi.org/10.1111/psyp.13016>
- Grinsted A, Moore JC, Jevrejeva S (2004) Application of the cross wavelet transform and wavelet coherence to geophysical time series. *Nonlinear Process Geophys* 11:561–566. <https://doi.org/10.5194/npg-11-561-2004>
- Gusnard DA, Raichle ME (2001) Searching for a baseline: functional imaging and the resting human brain. *Nat Rev Neurosci* 2:685–694. <https://doi.org/10.1038/35094500>
- Hagmann P, Cammoun L, Gigandet X et al (2008) Mapping the structural core of human cerebral cortex. *PLoS Biol* 6:e159. <https://doi.org/10.1371/journal.pbio.0060159>
- Haskell MW, Cauley SF, Bilgic B et al (2019) Network accelerated motion estimation and reduction (NAMER): convolutional neural network guided retrospective motion correction using a separable motion model. *Magn Reson Med* 82:1452–1461. <https://doi.org/10.1002/mrm.27771>
- Hassabis D, Maguire EA (2007) Deconstructing episodic memory with construction. *Trends Cogn Sci* 11:299–306. <https://doi.org/10.1016/j.tics.2007.05.001>
- Huang NE, Shen Z, Long SR et al (1998) The empirical mode decomposition and the Hilbert spectrum for nonlinear and non-stationary time series analysis. *Proc R Soc Lond Ser Math Phys Eng Sci* 454:903–995. <https://doi.org/10.1098/rspa.1998.0193>
- Klinger E, Cox WM (1987) Dimensions of thought flow in everyday life. *Imagin Cogn Personal* 7:105–128. <https://doi.org/10.2190/7K24-G343-MTQW-115V>
- Kramer MA, Cash SS (2012) Epilepsy as a disorder of cortical network organization. *Neuroscientist* 18:360–372. <https://doi.org/10.1177/1073858411422754>
- Krienen FM, Tu P-C, Buckner RL (2010) Clan mentality: evidence that the medial prefrontal cortex responds to close others. *J Neurosci* 30:13906–13915. <https://doi.org/10.1523/JNEUROSCI.2180-10.2010>
- Lange N, Zeger SL (1997) Non-linear fourier time series analysis for human brain mapping by functional magnetic resonance imaging. *J R Stat Soc Ser C* 46:1–29. <https://doi.org/10.1111/1467-9876.00046>
- Laufs H (2012) Functional imaging of seizures and epilepsy: evolution from zones to networks. *Curr Opin Neurol* 25:194–200. <https://doi.org/10.1097/WCO.0b013e3283515db9>
- Leech R, Sharp DJ (2014) The role of the posterior cingulate cortex in cognition and disease. *Brain* 137:12–32. <https://doi.org/10.1093/brain/awt162>
- Leech R, Kamourieh S, Beckmann CF, Sharp DJ (2011) Fractionating the default mode network: distinct contributions of the ventral and dorsal posterior cingulate cortex to cognitive control. *J Neurosci* 31:3217–3224. <https://doi.org/10.1523/JNEUROSCI.5626-10.2011>
- Leech R, Braga R, Sharp DJ (2012) Echoes of the brain within the posterior cingulate cortex. *J Neurosci* 32:215–222. <https://doi.org/10.1523/JNEUROSCI.3689-11.2012>
- Leonardi N, Richiardi J, Gschwind M et al (2013) Principal components of functional connectivity: a new approach to study dynamic brain connectivity during rest. *Neuroimage* 83:937–950. <https://doi.org/10.1016/j.neuroimage.2013.07.019>
- Liao W, Zhang Z, Pan Z et al (2010) Altered functional connectivity and small-world in mesial temporal lobe epilepsy. *PLoS One* 5:e8525. <https://doi.org/10.1371/journal.pone.0008525>
- Liu J, Liao X, Xia M, He Y (2018) Chronnectome fingerprinting: identifying individuals and predicting higher cognitive functions using dynamic brain connectivity patterns. *Hum Brain Mapp* 39:902–915. <https://doi.org/10.1002/hbm.23890>
- Lowe MJ (2010) A historical perspective on the evolution of resting-state functional connectivity with MRI. *Magn Reson Mater Phys Biol Med* 23:279–288. <https://doi.org/10.1007/s10334-010-0230-y>
- Mezer A, Yovel Y, Pasternak O et al (2009) Cluster analysis of resting-state fMRI time series. *Neuroimage* 45:1117–1125. <https://doi.org/10.1016/j.neuroimage.2008.12.015>
- Mitchell JP (2009) Social psychology as a natural kind. *Trends Cogn Sci* 13:246–251. <https://doi.org/10.1016/j.tics.2009.03.008>
- Moran JM, Kelley WM, Heatherton TF (2013) What can the organization of the brain's default mode network tell us about self-knowledge? *Front Hum Neurosci* 7:391. <https://doi.org/10.3389/fnhum.2013.00391>
- Murray RJ, Schaer M, Debbané M (2012) Degrees of separation: a quantitative neuroimaging meta-analysis investigating self-specificity and shared neural activation between self-and other-reflection. *Neurosci Biobehav Rev* 36:1043–1059. <https://doi.org/10.1016/j.neubiorev.2011.12.013>
- Ochsner KN, Ray RD, Cooper JC et al (2004) For better or for worse: neural systems supporting the cognitive down-and up-regulation of negative emotion. *Neuroimage* 23:483–499. <https://doi.org/10.1016/j.neuroimage.2004.06.030>

- Ochsner KN, Ludlow DH, Knierim K et al (2006) Neural correlates of individual differences in pain-related fear and anxiety. *Pain* 120:69–77. <https://doi.org/10.1016/j.pain.2005.10.014>
- Olsson A, Ochsner KN (2008) The role of social cognition in emotion. *Trends Cogn Sci* 12:65–71. <https://doi.org/10.1016/j.tics.2007.11.010>
- Oweis RJ, Abdulhay EW (2011) Seizure classification in EEG signals utilizing Hilbert–Huang transform. *Biomed Eng Online* 10:1–15. <https://doi.org/10.1186/1475-925X-10-38>
- Pearson JM, Heilbronner SR, Barack DL et al (2011) Posterior cingulate cortex: adapting behavior to a changing world. *Trends Cogn Sci* 15:143–151. <https://doi.org/10.1016/j.tics.2011.02.002>
- Peng ZK, Peter WT, Chu FL (2005) An improved Hilbert–Huang transform and its application in vibration signal analysis. *J Sound Vib* 286:187–205. <https://doi.org/10.1016/j.jsv.2004.10.005>
- Pittau F, Grova C, Moeller F et al (2012) Patterns of altered functional connectivity in mesial temporal lobe epilepsy. *Epilepsia* 53:1013–1023. <https://doi.org/10.1111/j.1528-1167.2012.03464.x>
- Qin P, Northoff G (2011) How is our self related to midline regions and the default-mode network? *Neuroimage* 57:1221–1233. <https://doi.org/10.1016/j.neuroimage.2011.05.028>
- Raichle ME, MacLeod AM, Snyder AZ et al (2001) A default mode of brain function. *Proc Natl Acad Sci* 98:676–682. <https://doi.org/10.1073/pnas.98.2.676>
- Richardson MP (2012) Large scale brain models of epilepsy: dynamics meets connectomics. *J Neurol Neurosurg Psychiatry* 83:1238–1248. <https://doi.org/10.1136/jnnp-2011-301944>
- Robertson HP (1929) The uncertainty principle. *Phys Rev* 34:163. [https://doi.org/10.1007/978-3-642-88213-5\\_2](https://doi.org/10.1007/978-3-642-88213-5_2)
- Salvador R, Suckling J, Schwarzbauer C, Bullmore E (2005) Undirected graphs of frequency-dependent functional connectivity in whole brain networks. *Philos Trans R Soc B* 360:937–946. <https://doi.org/10.1098/rstb.2005.1645>
- Schilbach L, Eickhoff SB, Mojzisch A, Vogeley K (2008) What's in a smile? Neural correlates of facial embodiment during social interaction. *Soc Neurosci* 3:37–50. <https://doi.org/10.1080/17470910701563228>
- Shimizu Y, Barth M, Windischberger C et al (2004) Wavelet-based multifractal analysis of fMRI time series. *Neuroimage* 22:1195–1202. <https://doi.org/10.1016/j.neuroimage.2004.03.007>
- Spreng RN, Mar RA, Kim AS (2009) The common neural basis of autobiographical memory, prospection, navigation, theory of mind, and the default mode: a quantitative meta-analysis. *J Cogn Neurosci* 21:489–510. <https://doi.org/10.1162/jocn.2008.21029>
- Stefan H, Lopes Da Silva FH (2013) Epileptic neuronal networks: methods of identification and clinical relevance. *Front Neurol* 4:8. <https://doi.org/10.3389/fneur.2013.00008>
- Stretton J, Winston GP, Sidhu M et al (2013) Disrupted segregation of working memory networks in temporal lobe epilepsy. *NeuroImage Clin* 2:273–281. <https://doi.org/10.1016/j.nicl.2013.01.009>
- Sun FT, Miller LM, D'Esposito M (2005) Measuring temporal dynamics of functional networks using phase spectrum of fMRI data. *Neuroimage* 28:227–237. <https://doi.org/10.1016/j.neuroimage.2005.05.043>
- Tang J, Zou Q, Tang Y et al (2007) Hilbert–Huang transform for ECG de-noising. *IEEE*, pp. 664–667. <https://doi.org/10.1109/ICBBE.2007.173>
- van den Heuvel MP, Mandl RC, Stam CJ et al (2010) Aberrant frontal and temporal complex network structure in schizophrenia: a graph theoretical analysis. *J Neurosci* 30:15915–15926. <https://doi.org/10.1523/JNEUROSCI.2874-10.2010>
- Vlooswijk MC, Jansen JF, de Krom MC et al (2010) Functional MRI in chronic epilepsy: associations with cognitive impairment. *Lancet Neurol* 9:1018–1027. [https://doi.org/10.1016/S1474-4422\(10\)70180-0](https://doi.org/10.1016/S1474-4422(10)70180-0)
- Vlooswijk MCG, Vaessen MJ, Jansen JFA et al (2011) Loss of network efficiency associated with cognitive decline in chronic epilepsy. *Neurology* 77:938–944. <https://doi.org/10.1212/WNL.0b013e31822cfc2f>
- Vogt BA, Vogt L, Laureys S (2006) Cytology and functionally correlated circuits of human posterior cingulate areas. *Neuroimage* 29:452–466. <https://doi.org/10.1016/j.neuroimage.2005.07.048>
- Wang J, Wang X, Xia M et al (2015) GRETNA: a graph theoretical network analysis toolbox for imaging connectomics. *Front Hum Neurosci* 9:386. <https://doi.org/10.3389/fnhum.2015.00386>
- Yaesoubi M, Allen EA, Miller RL, Calhoun VD (2015) Dynamic coherence analysis of resting fMRI data to jointly capture state-based phase, frequency, and time-domain information. *Neuroimage* 120:133–142. <https://doi.org/10.1016/j.neuroimage.2015.07.002>
- Yan C-G, Wang X-D, Zuo X-N, Zang Y-F (2016) DPABI: data processing & analysis for (resting-state) brain imaging. *Neuroinformatics* 14:339–351. <https://doi.org/10.1007/s12021-016-9299-4>
- Yang Z, Yang L, Qi D (2007) Detection of spindles in sleep EEGs using a novel algorithm based on the Hilbert–Huang transform. *Wavelet Anal Appl*. [https://doi.org/10.1007/978-3-7643-7778-6\\_40](https://doi.org/10.1007/978-3-7643-7778-6_40)
- Zhang Z, Liao W, Chen H et al (2011) Altered functional–structural coupling of large-scale brain networks in idiopathic generalized epilepsy. *Brain* 134:2912–2928. <https://doi.org/10.1093/brain/awr223>

**Publisher's Note** Springer Nature remains neutral with regard to jurisdictional claims in published maps and institutional affiliations.

Springer Nature or its licensor (e.g. a society or other partner) holds exclusive rights to this article under a publishing agreement with the author(s) or other rightsholder(s); author self-archiving of the accepted manuscript version of this article is solely governed by the terms of such publishing agreement and applicable law.